

Graphene oxide-modified polyaniline pigment for epoxy based anti-corrosion coatings

Vandana A. Mooss¹ · Abhijit A. Bhopale² · Pravin P. Deshpande² · Anjali A. Athawale¹

Received: 27 October 2016 / Accepted: 10 February 2017 / Published online: 18 February 2017
© Institute of Chemistry, Slovak Academy of Sciences 2017

Abstract In the present work, a set of polyaniline–graphene oxide (PANI–GO) nanocomposites which exhibit superior properties in terms of shelf life, processability and conductivity due to the synergistic effect of GO and PANI, have been synthesized by varying the concentration of highly non-conducting GO with respect to aniline. The obtained materials were characterized by UV–Vis, FTIR, XRD, Raman, TGA as well as FESEM, TEM analysis. The results reveal that nanocomposites show better dispersibility, crystallinity, thermal stability, and conductivity. Further, the synthesized composites have been tested for their anti-corrosion properties. The potentiodynamic results reveal that PANI nanocomposites with 1% GO exhibited long-term anti-corrosion behavior with a corrosion rate of $6.5 \times 10^{-5} \text{ mm year}^{-1}$, which is much lower than its individual components and commercial-grade red oxide. Also, it possesses highest impedance modulus $\sim 33 \text{ k}\Omega \text{ cm}^2$ and real impedance $\sim 32 \text{ k}\Omega \text{ cm}^2$, maximum coating resistance $\sim 14.81 \times 10^3 \Omega \text{ cm}^2$ and minimum coating capacitance after 96 h of immersion in 3.5% mass NaCl than those exhibited by all other coated samples. Higher concentration of GO could not retard the corrosion

rate confirming that hydrophilicity of GO play an important role in the redox mechanism of PANI.

Keywords Polyaniline · Graphene oxide · Nanocomposites · Anti-corrosion properties

Introduction

Among the conducting polymers, polyaniline has gained immense importance due to its ease of synthesis and relatively high level of electrical conductivity. It has been potentially used in diverse applications such as electrochemical devices (Lu et al. 2007; Athawale et al. 2006), chemical sensors (Marcel and Tarascon 2001), and also as anti-corrosion pigments (Deshpande et al. 2014). Inorganic hybrid-based coatings have been used widely for protecting metallic surfaces since the time of Deberry (1985); however, after the discovery of conducting polymers, PANI has been found to be an effective alternative for other conventional materials as anti-corrosion pigments (Williams and McMurray, 2005). While utilizing PANI as an effective pigment, one has to tailor its properties such as processability, environmental stability together with good adhesion to the substrate and integrity during synthesis. Several strategies have been adopted for enhancing its properties as well as anti-corrosion performance of PANI. The efficiency of PANI-pigmented vinyl acrylic coating on steel surface in neutral, acid, and alkaline media has been successfully reported for corrosion inhibition (Rohwerder and Michalik 2007; Sathiyarayanan et al. 2006). Alternatively, zinc-rich PANI primers have also been established (Meroufel et al. 2008). Furthermore, the performance of PANI anti-corrosion coating has been improved by the inclusion of other anti-corrosive agents in paints Kendova et al. 2008,

Electronic supplementary material The online version of this article (doi:10.1007/s11696-017-0146-3) contains supplementary material, which is available to authorized users.

✉ Pravin P. Deshpande
pravinpd@hotmail.com

✉ Anjali A. Athawale
agbed@chem.unipune.ac.in

¹ Department of Chemistry, Savitribai Phule Pune University, Pune 411007, MS, India

² Department of Metallurgy and Materials Science, College of Engineering, Shivajinagar, Pune 411005, MS, India

mostly in the macroparticulate form. In polymer based coatings, addition of various metal oxide nanoparticles like titanium oxide (TiO₂), zinc oxide (ZnO) and layered silicates (Radhakrishnan et al. 2009; Mostafaei and Nasirpour 2014; Olad and Naseri 2010) in PANI matrix is seen to render better resistance against electrochemical corrosion.

In the light of growing interest on the development of anti-corrosion paints, conductive graphene appears to be a good alternative for enhanced corrosion protection due to its lower density and higher aspect ratio protection (Chang et al. 2012; Yeh et al. 2014; Liu et al. 2014). To preclude the re-aggregation of graphene-related compounds, it has been mostly used in reduced form or by covalent functionalization with inorganic nano particles such as Al₂O₃ (He et al. 2015; Zhang et al. 2016; He et al. 2016). An effective nanopaint formulation has been reported by crosslinking graphene oxide with alkyd resin lipid chains for corrosion resistance as well as antibacterial applications (Krishnamoorthy et al. 2014). Thus, most of the reported procedures have adopted multistep modification for enhanced compatibility of graphene-based compounds in viable coatings. In the present work, we report the detailed investigation of PANI composite modified with as-synthesized graphene oxide as an anti-corrosion pigment on mild steel. In our previous work (Mooss and Athawale 2016), synthesis of a series of nanocomposites of PANI–GO with varying concentrations of GO and its effect on partial phase transition of polymer have been reported with a systematic study revealing the structure–property relationship between PANI and GO. Herein, attempts have been made to explore the efficacy of these materials as anti-corrosion pigments in epoxy matrix. The present investigation reports lowest corrosion rate for PANI with 1% of GO, which is much lower than the reported PANI–graphene composites.

Experimental

Materials

AR-grade graphite powder, potassium permanganate (KMnO₄), sulphuric acid–phosphoric acid (H₂SO₄–H₃PO₄), hydrogen peroxide (30% H₂O₂), aniline, sodium salt of dodecyl benzene sulfonic acid (SDBS), hydrochloric acid (HCl) and ammonium persulfate (APS) were purchased from SD-Fine (SDFCL) Chemicals. Aniline was purified by double distillation under vacuum, prior to use, and other chemicals were used as obtained.

Synthesis of graphene oxide (GO)

GO has been synthesized by modifying the precursor ratio and time used in the improved Hummers method. In brief, 1.5 g of pure graphite powder was added to 9.5:0.5 mixture

of concentrated H₂SO₄–H₃PO₄ with constant stirring. After the formation of a dark-green-colored solution, KMnO₄ (6 times to graphite) was added in portions with continuous stirring in a water bath (~40 °C) for 12 h. The resulting solution was diluted with 100 ml of double-distilled water followed by the addition of 3 ml of 30% H₂O₂ which led to a color change from dark brown to yellowish brown. The colloidal solution was filtered and dried in vacuum oven for 24 h at 40 °C.

PANI–GO nanocomposites

In situ emulsion polymerization was employed for the synthesis of PANI–GO nanocomposites. GO was suspended in 50 ml of distilled water containing SDBS (0.2 mmol) under sonication for half an hour to obtain a homogenous dispersion. Aniline (1 mmol) was dispersed in the above-mentioned solution at room temperature with vigorous stirring. The pH of the resulting solution was maintained at 3 by the addition of HCl. APS (1 mmol) solution was added to this solution and the mixture was continuously stirred for 3 h. The precipitate of emeraldine salt was separated by filtration. Similar procedure was adopted for the synthesis of polyaniline and composites with 1, 5, and 15 weight percentage of GO. In the text, the composites with 1, 5, and 15 wt% of GO are denoted as PG1, PG5, and PG15, respectively.

Preparation of paint

Paints based on conducting PANI as well as conducting PANI–GO composite have been prepared by adopting the technique developed by Samui et al. (2003). For preparing the paint, conducting PANI/PANI–GO composite (2 g) as a pigment, 12 g of xylene, 8 g of titanium dioxide (TiO₂) and 8 g of bis-(2-ethylhexyl) phthalate (di-octyl phthalate: DOP) were added to 70 g solution of epoxy resin [Standard GY 250 supplied by Huntsman Advanced Materials (India) Pvt Ltd., Andheri (East), Mumbai, 400 093, India]. The mixture was ball-milled for 16 h (Ball Mill supplied by Indo German Industries, Daman, India. Drive motor: Crompton Make, 2 HP, 1440 rpm, 415 V, 50 Hz). Titanium dioxide and di-octyl phthalate were added to the epoxy resin to improve the viscosity and elastic properties of paint. Xylene was used as a solvent for paint formulation. The paint was filtered through fine cotton and applied on the low-carbon steel samples (AISI 1015 supplied by Rajasthan steels, Pune, India) with the help of a film applicator. The coating was uniform on the entire surface having a thickness of ~60 μm. Finally, the painted low-carbon steel samples were cured in air at ambient temperature for 24 h.

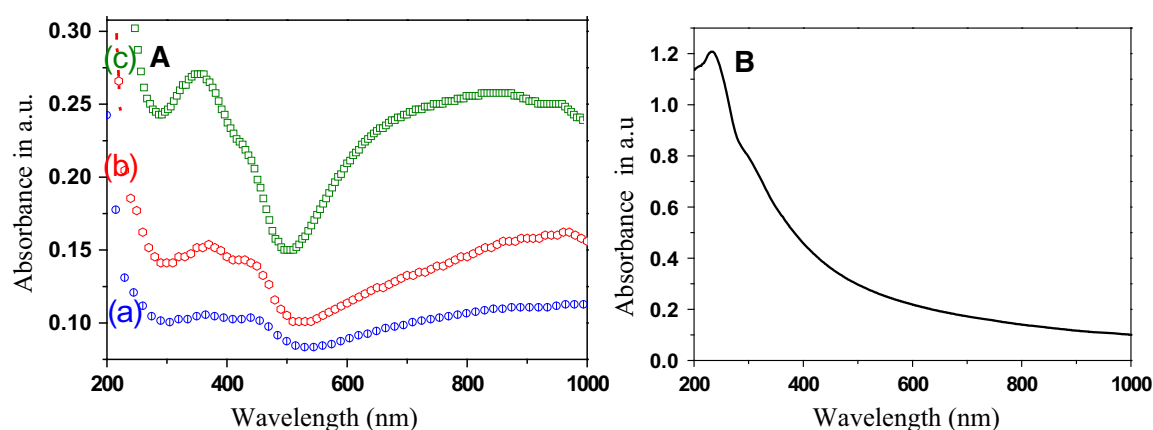


Fig. 1 UV-Vis spectra of **A** PG1, PG5, PG15 (a–c) and **B** GO

Characterization

UV-Vis absorption spectra were recorded on Shimadzu-1800 spectrophotometer between 200 and 1000 nm. FTIR analysis was performed on Bruker Tensor-37(ATR) spectrometer. X-ray diffractograms were recorded on a Bruker AXSD-8 advance X-ray diffractometer with monochromatic Cu-K α radiation ($k = 1.5406 \text{ \AA}$) in the 2θ range of $5\text{--}80^\circ$. Raman measurements were carried out using Renishaw's in Via laser Raman microscope with an excitation wavelength of 532 nm. Thermal analyses of the samples were carried out between 30 and 900 °C in nitrogen atmosphere at a heating rate of $10 \text{ }^\circ\text{C min}^{-1}$ using PerkinElmer TGA-4000. FESEM analyses of the samples were carried out on a FEI-Quanta 450 FEG instrument. Transmission electron microscope (TEM) images were recorded using a Tecnai G2 U-TWIN LaB6 (200 kV).

Corrosion studies

For corrosion studies, a three-electrode cell system was used with paint-coated sample as working electrode (8 cm^2), platinum as counter electrode and saturated calomel electrode (SCE; pH Products, Hyderabad, India) as a reference electrode in 3.5 mass% NaCl solution as electrolyte. The cell was coupled with Gamry reference system 1000 (Wilmington, USA) for electrochemical measurements. Tafel extrapolation method was used to determine the corrosion rate of the coated samples. In this technique, the polarization curves are obtained by applying a potential of $\pm 250 \text{ mV}$ with respect to open circuit potential. Resulting Tafel plots contain anodic and cathodic branches. Gamry software was used to determine the corrosion rate. Potentiodynamic impedance spectroscopy in the frequency range from 100 kHz to 0.001 Hz with an initial delay of 1800 s and 10 mV voltages was employed. All the measurements were carried out for five times to

obtain good reproducibility of the results. Impedance values are reproducible from ± 2 to 3%.

Results and discussion

Figure 1a depicts the UV-Vis absorption spectra of aqueous dispersions of PANI-GO composites, while Fig. 1b (inset) shows the optical spectrum of GO. Pure PANI is not dispersible in water, whereas the composites exhibit good dispersibility. The characteristic peak of GO is observed at 231 nm ($\pi\text{-}\pi^*$ transition) along with a shoulder at 300 nm ($n\text{-}\pi^*$ transition) (Lai et al. 2012). The spectra (Fig. 1a) of the polymer composites exhibit two predominant peaks at 350 (benzenoid) as well as 445 nm (quinoid) with an extended tail above 700 nm indicating the formation of conducting phase. Although the characteristic peak of GO is absent in the optical spectra of all of the composites, a comparison of the spectra reveals that varying concentrations of GO offer substantial change in the structure of polyaniline backbone. The slight red shift in the quinoid peak accounts for enhanced inter-chain interaction within composites in the presence of GO (Yang et al. 2009; Rana and Malik 2012). Further, it is worth to note that the peak intensities of both benzenoid and quinoid peaks are comparable at low GO concentration, whereas higher concentration of GO ($\leq 5\%$) causes a sharp increase in the absorbance of benzenoid peak along with the partial disappearance of quinoid peaks. Also, the hypsochromic shift in the extended tail at higher concentration of GO confirms the reduction in the number of charge carriers. Hence, the results infer that higher concentration of GO apparently diminishes the probability of $n\text{-}\pi^*$ transitions in PANI by virtue of bulky functional groups on the graphitic layer of GO.

The FTIR spectra of GO, PANI and the composites are given in Fig. 2. GO shows characteristic peaks owing to hydroxyl, carbonyl, physically adsorbed water, C–O and

epoxy functional groups (Fig. 2a) at 3400–3100, 1727, 1624, 1407, 1316, 1018 and 870 cm^{-1} (Venugopal et al. 2012). The peaks at 1559 and 1473 cm^{-1} in bare PANI are attributable to C=C stretch of quinoid as well as benzenoid units (Fig. 2b). The peak at 1105 and 1289 cm^{-1} corroborates –N=Q–N and C–N stretching vibrations of emeraldine salt phase (Wang et al. 2013; Mathew et al. 2013). On comparison with as-synthesized PANI, significant changes have been observed in the FTIR spectra of nanocomposites as evident from the following observations: (a) downshift as well as broadening of vibrational modes due to =N(+)–H units, (b) apparent decrease in the peak intensity of $\sim 1306 \text{ cm}^{-1}$ and (c) upshift in C=C stretch vibrations of quinoid units from 1478 to 1505 cm^{-1} (the peak positions are marked in the figure); they fortify the strong mode of interactions between PANI and GO (Valles et al. 2011) in the composites (Fig. 2c–e). Also, the higher concentration of GO corroborates the partial transformation of emeraldine to leucoemeraldine phase.

The XRD pattern of graphene oxide shows characteristic peak at $2\theta = 10^\circ$ (002) with an inter-planar distance of 8.8 Å (Fig. 3a) signifying higher degree of oxidation of graphitic layers (Stankovic et al. 2006). A small peak at 25° accounts for the un-oxidized graphitic layers. The X-ray diffractogram of PANI exhibits two peaks at $2\theta = 19.95^\circ$ and 25.25° corresponding to 100 plane of quinoid units and 110 plane of benzenoid units (Fig. 3b). In case of composites, the peaks are observed to be sharper and intense indicating higher degree of crystallinity due to enhanced interactions between GO and PANI (Fig. 3c–e) (Navarro et al. 2010; Krishna et al. 2009). It is also to be noted that up to 5% GO offers maximum crystallinity to the sample, whereas higher concentration of GO disturbs the lateral order in the crystallite sites of PANI.

The formation of PANI–GO composites is further confirmed from the Raman analysis. Figure 4 demonstrates the

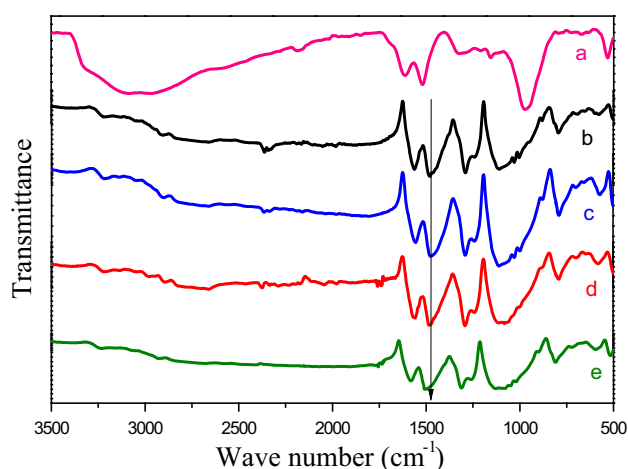


Fig. 2 FTIR spectra of a GO, b PANI, c PG1, d PG5, and e PG15

Raman spectra of the composites together with GO and PANI. GO exhibits characteristic peaks at 1356 and 1589 cm^{-1} corresponding to D and G bands as observed in Fig. 4a (Pimenta et al. 2007). Fig. 4b shows the Raman scattering at 1188, 1255, 1332, 1559 and 1618 cm^{-1} which can be attributed to the C–H, C–N, and C–N+, N–H and C–C vibrations of benzenoid ring as well as delocalized polarons of PANI, respectively (Sawangphruk et al. 2013). A comparison of the intensities of the Raman spectra of GO, PANI and the composites reveal sharp differences which are symbate with respect to the concentrations of GO. In case of composites, the peaks appear to be predominantly due to GO that can be assigned to the vibrational modes of GO as it is more Raman-active than PANI (Fig. 4). Also, the shift of $\sim 20 \text{ cm}^{-1}$ in the G band (which

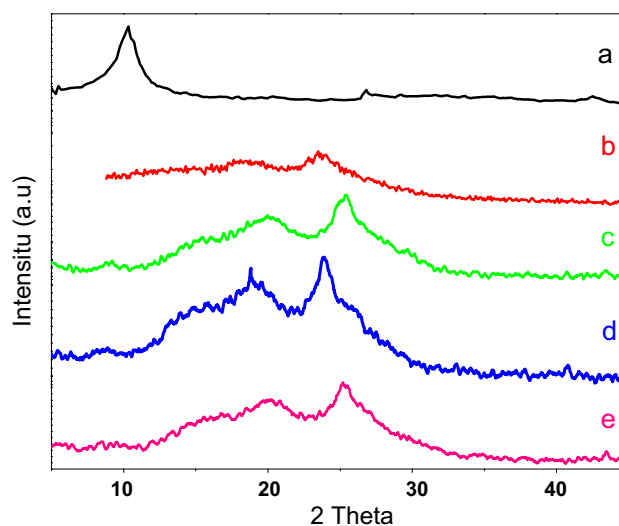


Fig. 3 XRD of a GO, b PANI, c PG1, d PG5, and e PG15

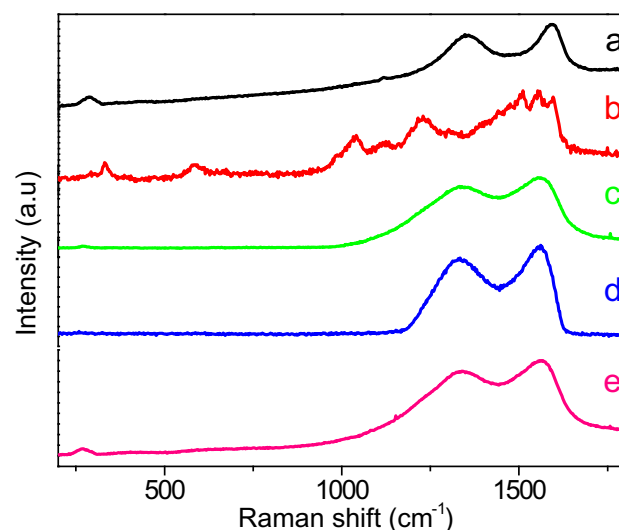


Fig. 4 Raman spectra of a GO, b PANI, c PG1, d PG5, and e PG15

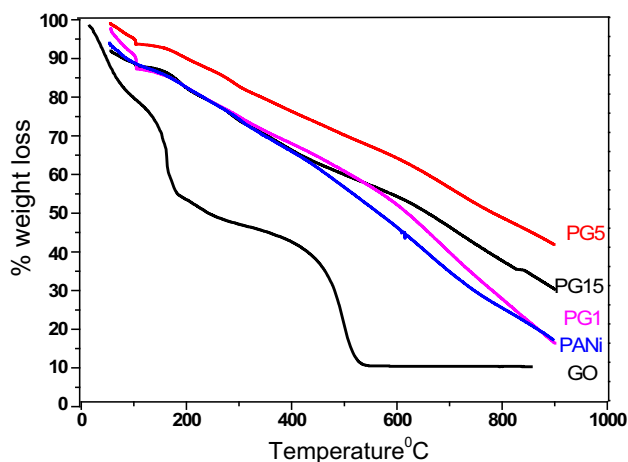


Fig. 5 Thermogravimetric analysis plots of GO, PANI, PG1, PG5, and PG15 composites

is higher in magnitude as reported in the literature) further supports the fact that due to the strong mode of interactions between PANI and GO, the electron pair on the nitrogen atom of PANI probably resonates with the adjacent benzene units of GO (Shao et al. 2014; Hsiao et al. 2010; Sahoo et al. 2013). Similarly, the ID/IG ratio is observed to

be lower for the composites in comparison to GO (Guo et al. 2012; Lee et al. 2009). Hence, it is evident that in the presence of GO in the composite, higher degree of interactions occur between PANI and GO apart from hydrogen bonding and π - π interactions owing to enhanced properties.

Thermal behavior of the samples was evaluated with the help of thermogravimetric analysis. GO is highly thermally unstable (Fig. 5) showing $\sim 91\%$ loss up to ~ 530 °C with a three-step loss. The initial two stages (up to 93 °C and 93–193 °C) being subsequent and sharp were followed by a third sharp step starting with a gradual loss (193–450, 450–530 °C). The initial two weight losses (20 and 26%) can be attributed to the loosely bound or physically adsorbed water molecules and acidic residues, respectively. While in the third step, degradation is due to both, the removal of by-products and C=O species till 530 °C (Ganguly et al. 2011). On the contrary, thermal stability of PANI is found to be significantly higher as compared to GO with two-step degradation. The initial small weight loss up to 10% can be accounted for the loss of adsorbed moisture or the release of solvent molecules (Liu et al. 2004). The second step involves gradual loss from 140 to 850 °C by virtue of the loss of mineral acid dopant

Fig. 6 FESEMs of **a** GO, **b** PANI, **c** PG1, **d** PG5, and **e** PG15

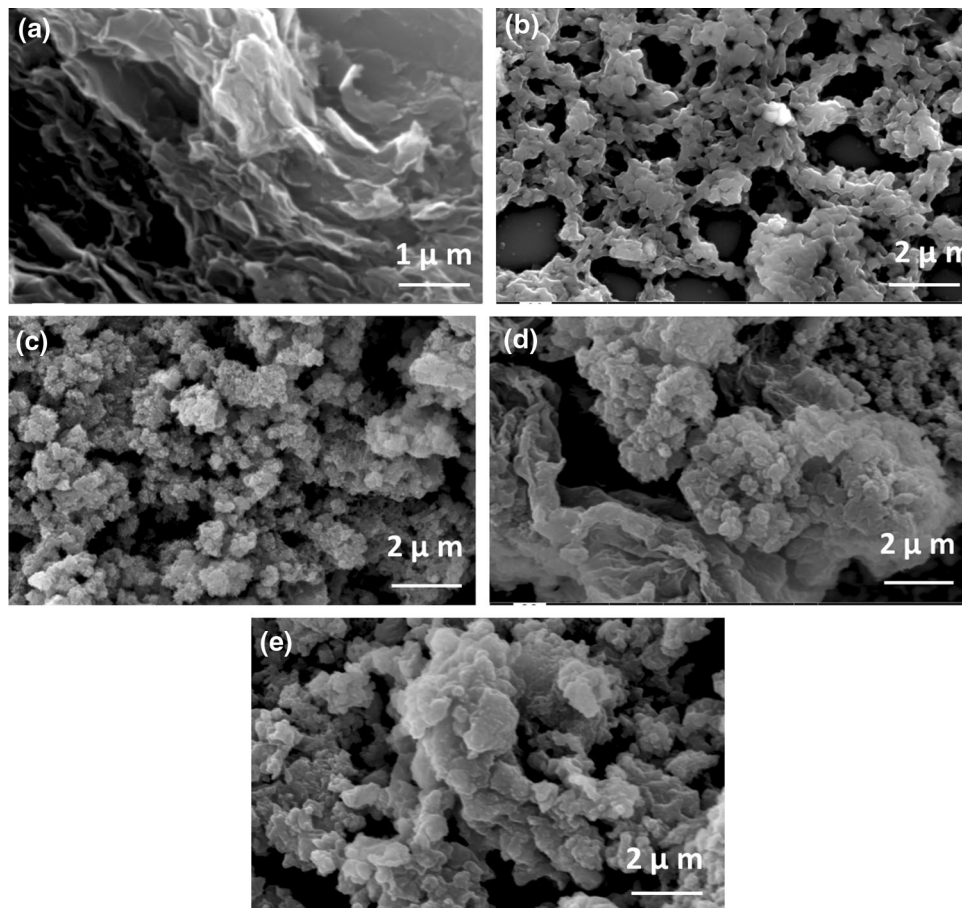


Fig. 7 TEMs of **a** GO, **b** PG1, **c** PG5, and **d** PG15

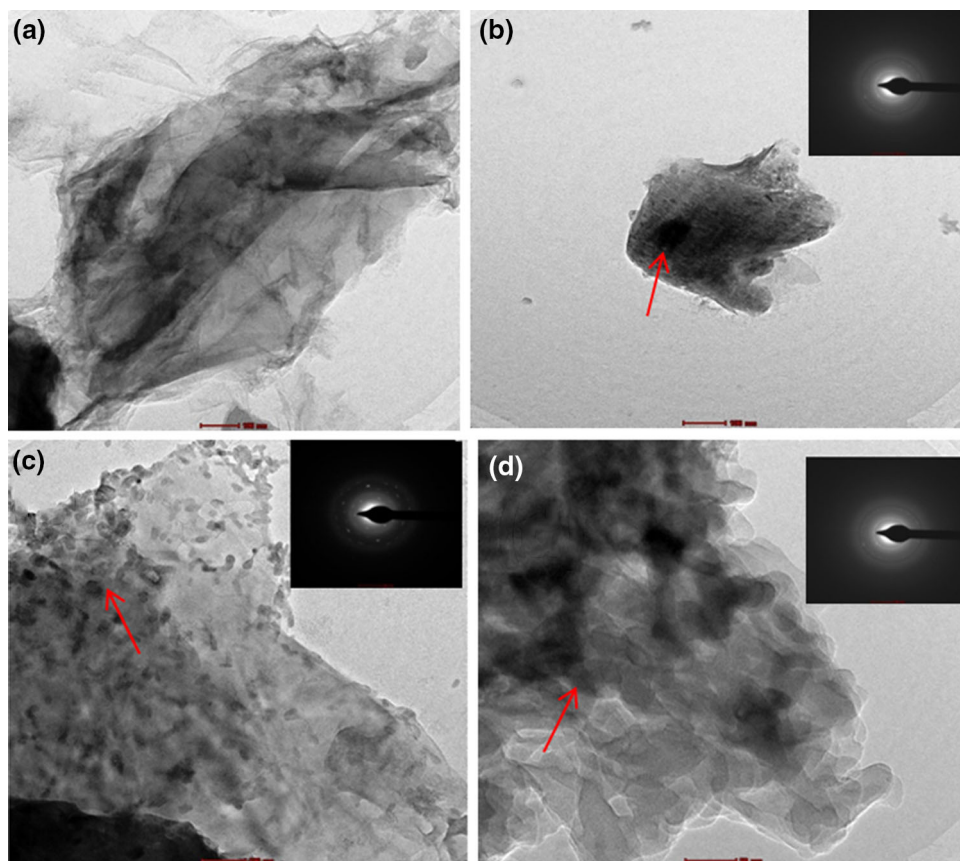


Fig. 8 Tafel plot for uncoated low-carbon steel (*thick trace*) and red oxide-coated low-carbon steel (*thin trace*) in 3.5 mass% NaCl solution

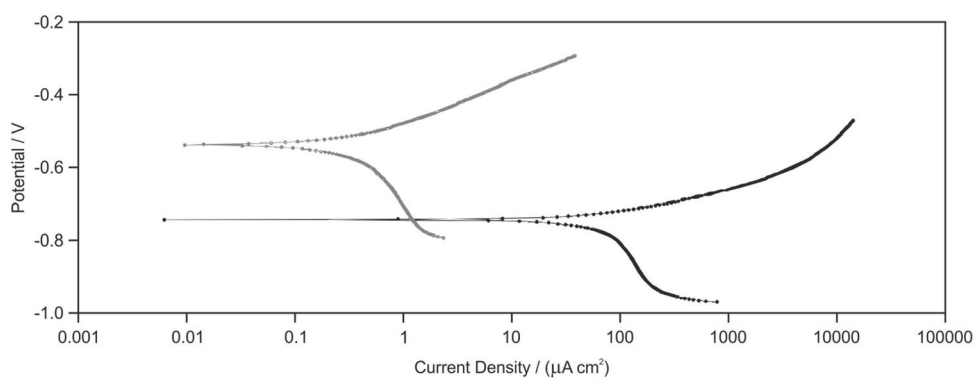


Fig. 9 Tafel plot for low-carbon steel coated with PANI-based paint (*thick trace*) and epoxy without pigment-coated (*thin trace*) low-carbon steel in 3.5 mass% NaCl solution

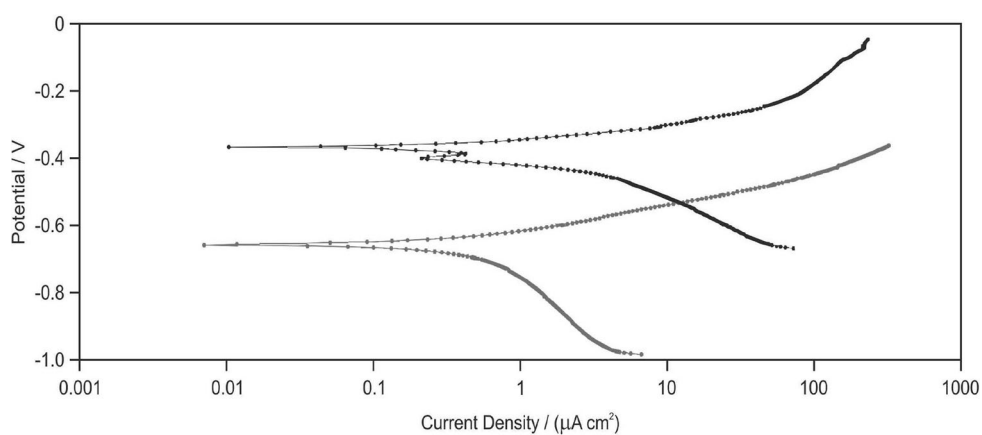


Fig. 10 Tafel plot for low-carbon steel coated with PG1 (*thin trace*) and PG5 (*thick trace*)-coated low-carbon steel in 3.5 mass% NaCl solution

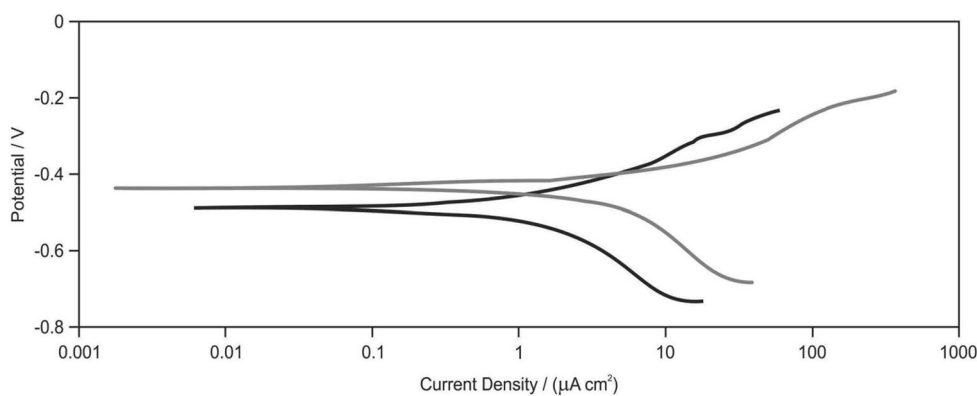


Fig. 11 Tafel plot for low-carbon steel coated with graphene oxide (*thick trace*) and PG15 composite based painted (*thin trace*) low-carbon steel in 3.5 mass% NaCl solution

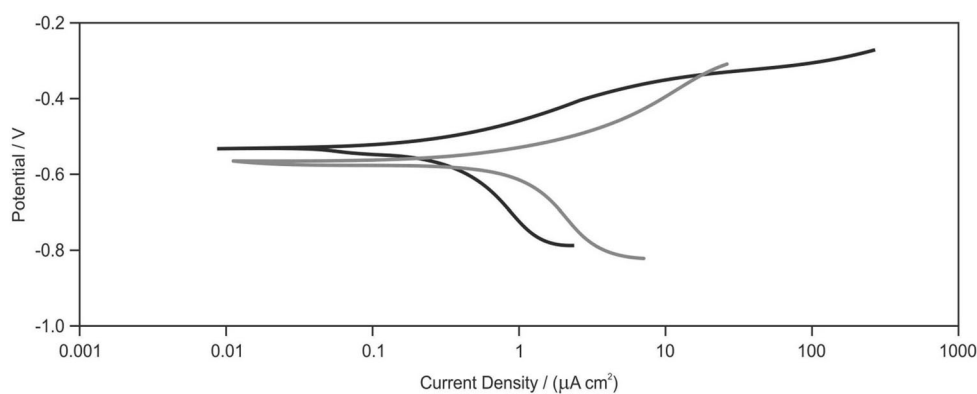


Table 1 Corrosion rates for uncoated and coated samples in 3.5 mass% NaCl solution

| Sample | E_{corr} (mV) | I_{corr} ($\mu\text{A cm}^{-2}$) | Corrosion rate (mm year^{-1}) |
|---|------------------------|---|--|
| Low-carbon steel | -731 | 70.30 | 2×10^{-1} |
| PANI-coated low-carbon steel | -390 | 9.04 | 2×10^{-2} |
| PG1-coated low-carbon steel | -410 | 0.26 | 6.5×10^{-5} |
| PG5-coated low-carbon steel | -570 | 0.67 | 1.05×10^{-4} |
| PG15-coated low-carbon steel | -590 | 0.97 | 2.5×10^{-4} |
| Graphene oxide-coated low-carbon steel | -550 | 0.40 | 7.2×10^{-5} |
| Red oxide-coated low-carbon steel | -560 | 0.43 | 7×10^{-5} |
| Epoxy-coated (without pigment) low-carbon steel | -640 | 3.25 | 4.9×10^{-2} |

molecules followed by the degradation of polymer backbone. The thermal stability of all of the composites is observed to be higher compared to the individual constituents, i.e., PANI and GO (Fig. 5). All the composites exhibit similar degradation pattern; however, the second degradation step is seen to be shifted towards higher temperature which may be due to high mode of interactions between GO and PANI in the composites. It is also worth noting that PG5 exhibits highest thermal stability with a loss of $\sim 60\%$ at $\sim 850^\circ\text{C}$. Conversely, at higher concentrations of GO, thermal stability is observed to decrease with a total loss up to 70% at similar temperature. These results can be correlated to the results of XRD, where composite with 15% GO exhibits lower crystallinity.

The micrographs of the samples are depicted in Fig. 6. GO (Fig. 6a) exhibits thin exfoliated nano sheets with distinct edges, whereas PANI shows nanosized globules which are inter-connected with each other. From Fig. 6c–e, one can observe significant change in morphology as a function of GO concentration when compared to its parent compounds. At lower concentration, one can see the predominance of spherical particles, whereas at higher concentrations of GO, template effect preferably increases the planarity of polymer particles. The degree of agglomeration also appears to be increased due to the stronger surface interactions facilitated by the functional groups present on the GO. Although, π - π interactions between GO and PANI backbone would result in

Fig. 12 Bode plot for polyaniline-coated low-carbon steel, just after immersion, and after 1, 2, 3 and 4 days of immersion in 3.5 mass% NaCl solution

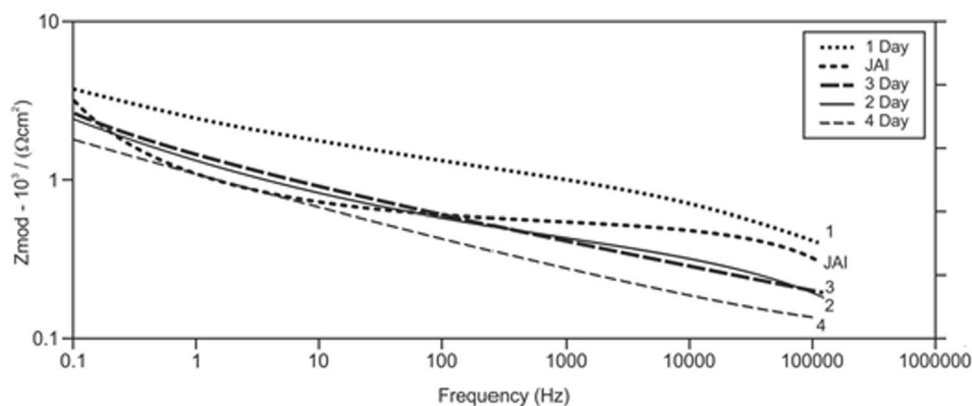


Fig. 13 Bode plot for PG1-based coated low-carbon steel, just after immersion (JAI), and after 1, 2, 3, and 4 days of immersion in 3.5 mass % NaCl solution

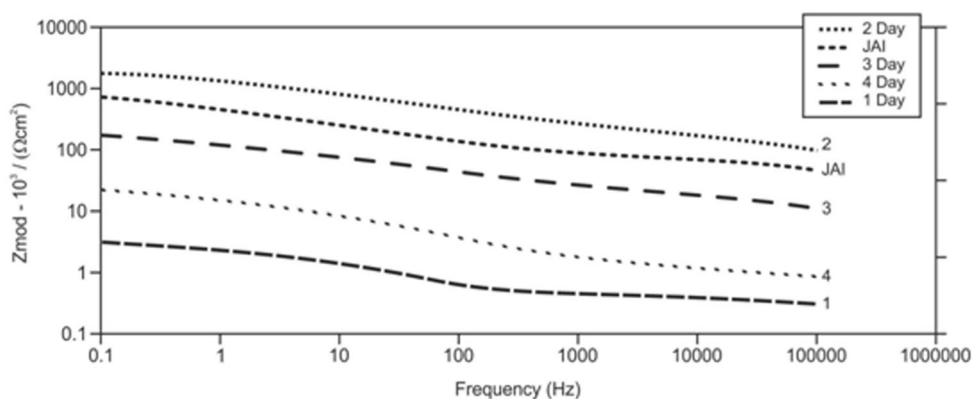
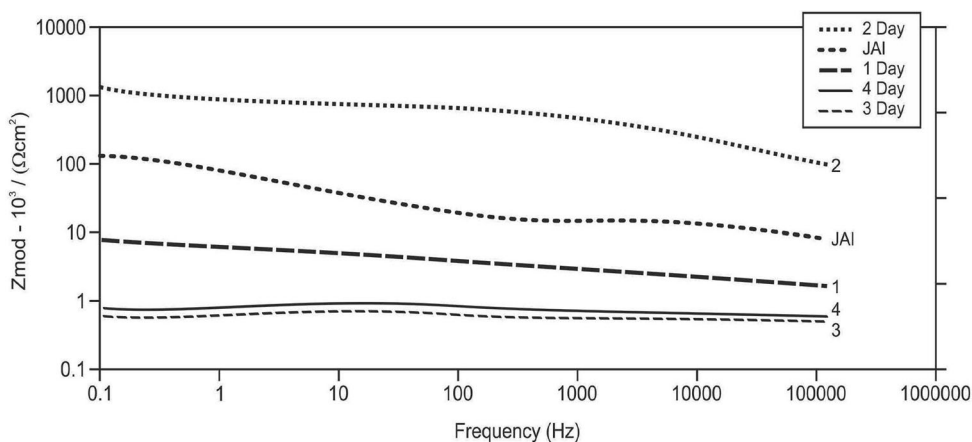


Fig. 14 Bode plot for PG5-based coated low-carbon steel, just after immersion, and after 1, 2, 3, and 4 days of immersion in 3.5 mass% NaCl solution



agglomeration, the size of the particles is in nanometer regime. It is expected that, the difference in the morphology and size of the nanoparticles also contribute to the corrosion protection mechanism (Mostafaei and Nasirpouri 2014; Yu et al. 2014).

The interactions between PANI and GO are further supported with the TEM analysis of selected samples. Figure 7 shows the TEM micrographs of GO, PG1, PG5, and PG15 samples. Multilayer lamellar sheets of GO can

be observed in Fig. 7a, whereas PANI and GO are clearly distinguishable in the composites, Fig. 7b–d. Also, it is evident from the micrographs of the composites that agglomeration in PANI (observed in FEG-SEM) basically consists of PANI particles with size distribution varying between 10 and 60 nm. These micrographs further justify the template effect of GO at higher concentrations and the polycrystalline nature of PANI–GO composites (SAED patterns shown as inset).

Potentiodynamic polarization studies

The corrosion rates were measured in 3.5 mass% NaCl solution using Tafel analysis. Tafel curves generated by scanning potential from E_{corr} to 250 mV (cathodic/anodic) for uncoated as well as coated samples are depicted in Figs. 8, 9, 10 and 11. The Tafel curves were analyzed using Gamry Echem Analyst. The values of corrosion potential, corrosion current density and corrosion rate presented in Table 1 were obtained after Tafel fitting with the help of software.

As observed from the table, the corrosion potential is seen to increase from -731 mV for uncoated low-carbon steel to more positive values as -390 , -410 , -570 , -590 , -550 , -560 , and -640 mV in PANI, PG1, PG5, PG15, GO, red oxide and epoxy-coated low-carbon steel samples, respectively. The shift in positive direction suggests that the low-carbon steel substrates are restored in 3.5 mass% NaCl by anodic protection in presence of coatings due to the prevention of the cathodic reaction process. It is seen that the corrosion rate is substantially reduced due to

decrease in current density from $70.3 \mu\text{A cm}^{-2}$ to 9.04, 0.26, 0.97, 0.40, 0.43 and 3.25 in PANI, PG1, PG5 and PG15, GO, red oxide and epoxy-coated low-carbon steel, respectively. The corrosion rates, in 3.5% mass NaCl solution, are found to be 2×10^{-1} , 2×10^{-2} , 6.5×10^{-5} , 1.05×10^{-4} , 2.5×10^{-4} , 7.2×10^{-5} , 7×10^{-5} and 4.9×10^{-2} in PANI, PG1, PG5, PG15, GO, red oxide and epoxy-coated low-carbon steel samples, respectively. Among all the samples, PG1 is seen to exhibit the lowest corrosion rate. However, corrosion rate increases with increase in GO concentration. This effect can be attributed to the hydrophilic nature of graphene oxide. The hydrophilicity of the pigment accelerates the rate of electrochemical reactions which causes corrosion (Conradi and Kocijan 2016).

Electrochemical impedance spectroscopy

Electrochemical impedance spectroscopic studies were carried out in 3.5 mass% NaCl solution and are reported here in terms of Bode plots as depicted in Figs. 12, 13, 14,

Fig. 15 Bode plot for PG15-coated low-carbon steel, just after immersion, and after 1, 2, 3, and 4 days of immersion in 3.5 mass% NaCl solution

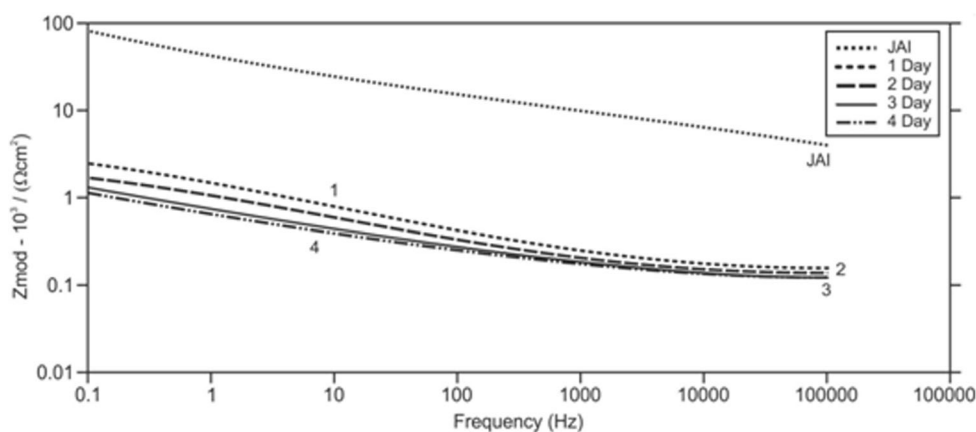


Fig. 16 Bode plot for graphene oxide-coated low-carbon steel, just after immersion and after 1, 2, 3, and 4 days of immersion in 3.5 mass% NaCl solution

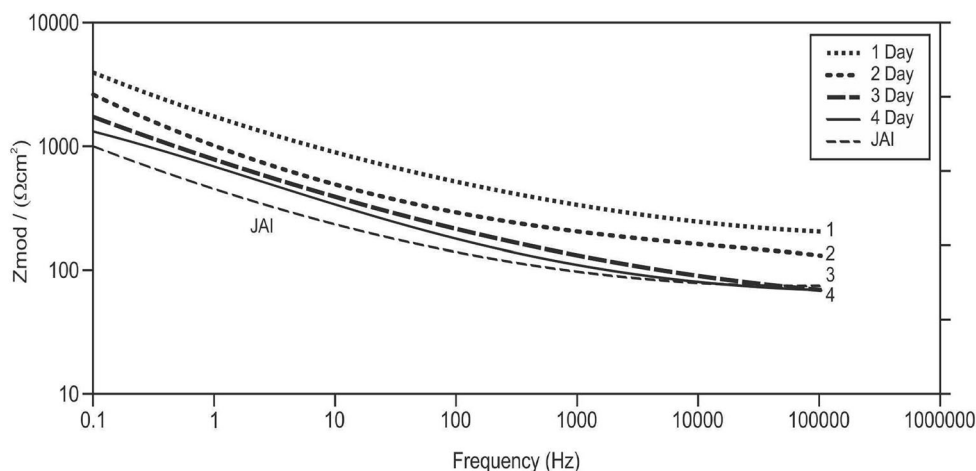


Fig. 17 Bode plot for red oxide-painted steel, just after immersion, and after 1, 2, 3, and 4 days of immersion in 3.5 mass% NaCl solution

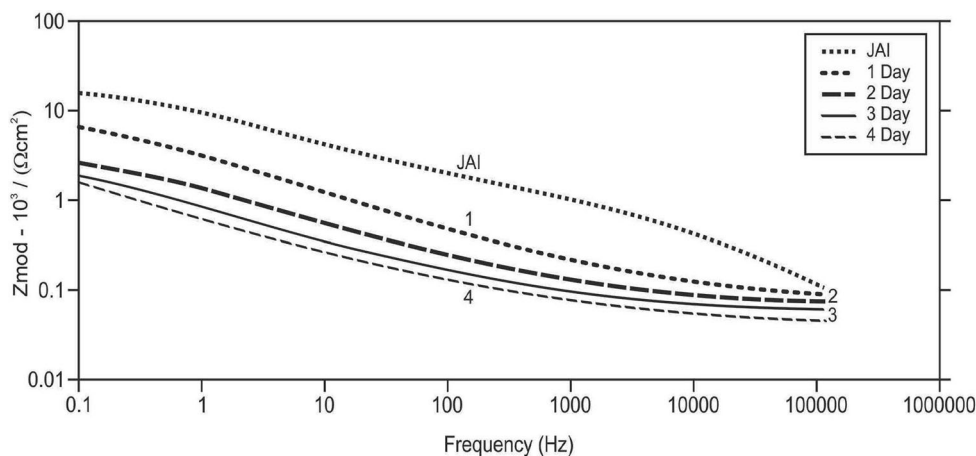
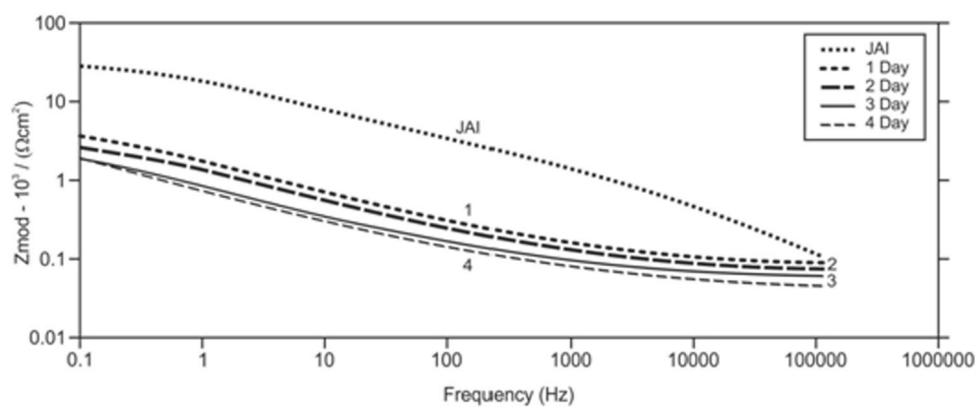


Fig. 18 Bode plot for low-carbon steel and epoxy coated (without pigment) low-carbon steel, just after immersion, and after 1, 2, 3, and 4 days of immersion in 3.5 mass% NaCl solution



15, 16, 17 and 18. These plots are modeled using equivalent circuit shown in Fig. 19; the impedance values, coating resistance and capacitance are included in Tables 2 and 3, respectively.

In case of PANI-coated low-carbon steel, increase in the impedance values (Z_{mod} and Z_{real}) from 3.18 to 3.79 and 2.29 to 3.62 $\text{k}\Omega\text{-cm}^2$, respectively, is observed in the time period between just after immersion and 24 h of immersion; this indicates the protective property of the PANI coating (Table 2). However, continuous decrease in the impedance values (Z_{mod} and Z_{real}), from 2.63 and 1.78 $\text{k}\Omega\text{-cm}^2$ after 24 h of immersion to 2.42 to 1.73 $\text{k}\Omega\text{-cm}^2$ after 96 h of immersion reveals coating degradation. Similarly, PG1- and PG5-coated samples also show an increase in the impedance values up to 48 h of immersion followed by a decrease in the impedance values up to 96 h of immersion as noted from Table 2. However, in case of PG1 sample, higher impedance value by the end of 96 h of immersion (33 $\text{k}\Omega\text{-cm}^2$), as compared to PG5 sample, reveals better protective properties of PG1-coated sample than PG5-coated sample. Further, in case of PG15-coated sample, a gradual decrease in the impedance values (83–0.59 and 78–0.52 $\text{k}\Omega\text{-cm}^2$), from just after immersion up to 96 h of

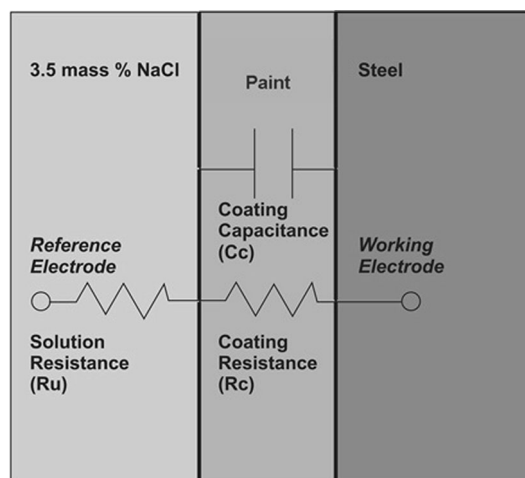


Fig. 19 Equivalent circuit used for modeling impedance curves

immersion, is observed. In case of GO-coated sample, a negligible increase is observed in the impedance values up to 24 h followed by a gradual decrease at higher time intervals up to 96 h. The red oxide-coated and epoxy without pigment-coated samples, also exhibit a continuous decrease in the impedance values as a function of

Table 2 Impedance parameters

| Sample | Immersion time (h) | Z_{mod} ($\text{k}\Omega\text{-cm}^2$) | Z_{real} ($\text{k}\Omega\text{-cm}^2$) |
|--|----------------------|---|--|
| PANI-painted low-carbon steel | Just after immersion | 3.18 | 2.29 |
| | 24 | 3.79 | 3.62 |
| | 48 | 2.63 | 2.42 |
| | 72 | 2.39 | 2.31 |
| | 96 | 1.78 | 1.73 |
| PG1-painted low-carbon steel | Just after immersion | 814 | 593 |
| | 24 | 5.13 | 4.94 |
| | 48 | 1499 | 1422 |
| | 72 | 181 | 177 |
| | 96 | 33 | 32 |
| PG5-painted low-carbon steel | Just after immersion | 124 | 119 |
| | 24 | 9.56 | 9.26 |
| | 48 | 2008 | 2040 |
| | 72 | 0.82 | 0.75 |
| | 96 | 0.85 | 0.81 |
| PG15-painted low-carbon steel | Just after immersion | 83 | 78 |
| | 24 | 1.43 | 1.26 |
| | 48 | 0.87 | 0.75 |
| | 72 | 0.67 | 0.59 |
| | 96 | 0.59 | 0.52 |
| GO-painted low-carbon steel | Just after immersion | 1 | 0.69 |
| | 24 | 4.1 | 3.54 |
| | 48 | 2.45 | 2.18 |
| | 72 | 2.04 | 1.92 |
| | 96 | 1.78 | 1.64 |
| Red oxide-painted low-carbon steel | Just after immersion | 21.83 | 19.47 |
| | 24 | 8.46 | 6.68 |
| | 48 | 5.66 | 4.35 |
| | 72 | 4.12 | 3.18 |
| | 96 | 3.15 | 2.54 |
| Without pigment painted low-carbon steel | Just after immersion | 29.33 | 28 |
| | 24 | 3.31 | 3.06 |
| | 48 | 2.29 | 2.22 |
| | 72 | 1.58 | 1.50 |
| | 96 | 1.56 | 1.48 |

immersion time. These results reveal the ingress of corrosive species and, thereby, also coating degradation. Thus, PG1-coated sample exhibits the best corrosion protection as compared to all other samples in 3.5 mass % NaCl solution. The values of coating resistance and coating capacitance (calculated from equivalent circuit and the values are given in Table 3 and Nyquist plots are not given) for PG1 are found to be $\sim 730.2 \times 10^3 \Omega\text{-cm}^2$ (maximum) and $\sim 6.98 \times 10^{-3} \mu\text{F}$ (minimum), respectively, after 48 h of immersion in 3.5% mass NaCl solution. Maximum coating resistance indicates highest protective ability of PG1-type coating and lower coating

capacitance reveals minimum water uptake during 48 h of immersion. Even after 96 h of immersion in 3.5% mass NaCl, the values of coating resistance $\sim 14.81 \times 10^3 \Omega\text{-cm}^2$ and coating capacitance, in case of PG1 sample $\sim 628 \times 10^{-3} \mu\text{F}$, are found to be maximum and minimum, respectively, than those exhibited by all other coated samples (Table 3). It can, therefore, be said that PG1-coated sample exhibits better corrosion resistance compared to all other samples in 3.5 mass% NaCl solution.

Thus, impedance spectroscopic results support potentiodynamic studies (Table 1). Wessling (1996) and Lu et al. (1995) demonstrated that when doped PANI is placed

Table 3 Coating resistance and capacitance as obtained from Nyquist plots

| Sample | Immersion time (h) | R ($\Omega\text{-cm}^2$) | C (μF) |
|--|----------------------|------------------------------|-----------------------|
| PANI-painted low-carbon steel | Just after immersion | 2.73×10^3 | 314.5 |
| | 24 | 1.02×10^3 | 0.14 |
| | 48 | 639.8 | 1.37 |
| | 72 | 459.3 | 87.48 |
| | 96 | 642.7 | 8.13 |
| PG1-painted low-carbon steel | Just after immersion | 301.6×10^3 | 0.030 |
| | 24 | 2.34×10^3 | 4.91 |
| | 48 | 730.2×10^3 | 0.006 |
| | 72 | 52.80×10^3 | 0.017 |
| | 96 | 14.81×10^3 | 0.62 |
| PG5-painted low-carbon steel | Just after immersion | 42.35×10^3 | 0.138 |
| | 24 | 4.09×10^3 | 3.82 |
| | 48 | 34.75×10^3 | 0.009 |
| | 72 | 386.5 | 14.50 |
| | 96 | 428.3 | 82 |
| PG15-painted low-carbon steel | Just after immersion | 18.72×10^3 | 0.163 |
| | 24 | 494.0 | 14.90 |
| | 48 | 295.2 | 22.27 |
| | 72 | 238.2 | 47.77 |
| | 96 | 220.8 | 60.81 |
| GO-painted low-carbon steel | Just after immersion | 426.5 | 319.2 |
| | 24 | 1.55×10^3 | 29.40 |
| | 48 | 916.4 | 29.24 |
| | 72 | 815.6 | 21.69 |
| | 96 | 732.3 | 40.95 |
| Red oxide-painted low-carbon steel | Just after immersion | 5.15×10^3 | 1.30 |
| | 24 | 2.76×10^3 | 17.80 |
| | 48 | 2.04×10^3 | 33.06 |
| | 72 | 1.84×10^3 | 63.01 |
| | 96 | 1.52×10^3 | 84.03 |
| Without pigment painted low-carbon steel | Just after immersion | 2.77×10^3 | 0.074 |
| | 24 | 1.44×10^3 | 27.06 |
| | 48 | 1.11×10^3 | 34.26 |
| | 72 | 653.7 | 51.38 |
| | 96 | 691.7 | 63.72 |

in contact with steel, the steel surface undergoes rapid oxidation to provide a layer of iron oxide at the PANI–steel interface. In the present investigations, increased impedance values in case of PANI-coated sample from just after immersion to 24 h of immersion and in case of PG1- and PG5-coated sample between 24 and 48 h of immersion can be assigned to the formation of passive iron oxide layer. However, this beneficial effect is not seen in case of PG15 sample due to increased concentration of GO. GO, being hydrophilic in nature, permits water intake during immersion and is, thus, responsible for coating degradation as a function of immersion time.

Conclusions

The conducting PANI–GO nanocomposites exhibit superior crystallinity, processability, environmental stability, and thermal stability as compared to its parental compounds. The corrosion protection properties of PANI–GO composites-painted low-carbon steel in 3.5 mass% NaCl solution are investigated by potentiodynamic tests and electrochemical impedance spectroscopy. Among the composites, PG1-painted low-carbon steel possesses lowest corrosion rate as compared to that of PG5- and PG15-painted low-carbon steels in 3.5 mass% NaCl. Novelty of

the composite paint coating lies in the enhancement of corrosion protection of low-carbon steel by simultaneously operating mechanisms viz. barrier effect and protection due to the redox properties of PANI in presence of low concentration of GO.

Acknowledgements The authors thank Department of Chemistry and Physics for characterization techniques. One of the authors VM thanks SPPU for the financial support. The authors also thank Prof. N.B. Dhokey, Head, Department of Metallurgy and Materials Science, College of Engineering, Pune, 411005 (M.S.), India, for providing facilities for anti-corrosion studies and Prof. B.B. Ahuja, Director, College of Engineering, Pune, 411005 (M.S.), India, for his encouragement.

References

- Athawale A, Bhagwat SV, Katre P (2006) Nanocomposite of Pd-polyaniline as a selective methanol sensor. *Sensors Actuators B* 114:263–267. doi:10.1016/j.snb.2005.05.009
- Chang CH, Huang TC, Peng CW, Yeh TC, Lu HI, Hung WI, Weng CJ, Yang TI, Yeh JM (2012) Novel anticorrosion coatings prepared from polyaniline/graphene composites. *Carbon* 50:5044–5051. doi:10.1016/j.carbon.2012.06.043
- Conradi M, Kocijan A (2016) Surface and anticorrosion properties of hydrophobic and hydrophilic TiO₂ coatings on a stainless-steel substrate (2016). *Mat Technol* 50(6):967–970. DOI:10.17222/mit.2016.068
- Deberry DW (1985) Modification of the electrochemical and corrosion behavior of stainless steel with electroactive coating. *J Electrochem Soc* 132:1022–1026. doi:10.1149/1.2114008
- Deshpande PP, Jadhav NG, Gelling VJ, Sazou D (2014) Conducting polymers for corrosion protection: a review. *J Coating Technol Res* 11:473–494. doi:10.1007/s11998-014-9586-7
- Ganguly A, Sharma S, Papakonstantinou P, Hamilton J (2011) Probing the thermal deoxygenation of graphene oxide using high-resolution in situ X-ray-based spectroscopies. *J Phys Chem C* 115:17009–17019. doi:10.1021/jp203741y
- Guo Y, Sun X, Liu Y, Wang W, Qiu H, Gao J (2012) One pot preparation of reduced graphene oxide (RGO) or Au (Ag) nanoparticle-RGO hybrids using chitosan as a reducing and stabilizing agent and their use in methanol electro oxidation. *Carbon* 50:2513–2523. doi:10.1016/j.carbon.2012.01.074
- He Y, Yu Z, Di H, Ma Y, Liang L, Pan Y, Zhang C (2015) Fabrication of graphene oxide–alumina hybrids to reinforce the anti-corrosion performance of composite epoxy coatings. *Appl Surf Sci* 351:986–996. doi:10.1016/j.apsusc.2015.06.026
- He Y, Yu Z, Liang L, Ma Y, Di H (2016) Covalent modification of graphene oxide by metronidazole for reinforced anti-corrosion properties of epoxy coatings. *RSC Adv* 6:18217–18226. doi:10.1039/C5RA23595B
- Hsiao MC, Liao SH, Yen MY, Liu PI, Pu NW, Wang CA, Ma CCM (2010) Preparation of covalently functionalized graphene using residual oxygen-containing functional groups. *ACS App Mater Interfaces* 2:3092–3099. doi:10.1021/am100597d
- Kendova A, Vesely D, Stejskal J (2008) Organic coatings containing polyaniline and inorganic pigments as corrosion inhibitors. *Prog Organ Coating* 62:105–116. doi:10.1016/j.porgcoat.2007.10.001
- Krishna BM, Saha A, Okram GS, Soni A, Purakayastha S, Ghosh B (2009) Electrical properties of polyaniline doped with metal ions. *J Phys D Appl Phys* 42:095404–095410. doi:10.1088/0022-3727/42/9/095404
- Krishnamoorthy K, Jeyasubramanian K, Premanathan M, Subbiah G, Shin HS, Kim SJ (2014) Graphene oxide nanopaint. *Carbon* 7(2):328–337
- Lai Q, Zhu S, Luo X, Zou M, Huang S (2012) Ultraviolet-visible spectroscopy of graphene oxides. *AIP Advances* 2(32146):1–6. doi:10.1063/1.4747817
- Lee V, Whittaker L, Jaye C, Baroudi KM, Fischer DA, Banerjee S (2009) Large-area chemically modified graphene films: electrophoretic deposition and characterization by soft x-ray absorption spectroscopy. *Chem Mater* 21:3905–3916. doi:10.1021/cm901554p
- Liu P, Liu W, Xue Q (2004) In situ chemical oxidative graft polymerization of aniline from silica nanoparticles. *Mater Chem Phys* 87:109–113. doi:10.1016/j.matchemphys.2004.05.001
- Liu WR, Chang KC, Ji WF, Lai MC, Hsiao YR, Hsu CH, Chuang TL, Wei Y, Yeha JM (2014) Synergistic effects of hydrophobicity and gas barrier properties on the anticorrosion property of PMMA nanocomposite coatings embedded with graphene nanosheets. *Polym Chem* 5:1049–1056. doi:10.1039/C3PY01178J
- Lu WK, Elsenbaumer RL, Wessling B (1995) Corrosion protection of mild steel by coating containing polyaniline. *Synth Met* 71:2163–2166. doi:10.1016/0379-6779(94)03204-J
- Lu JX, Moon KS, Wong CP (2007) High dielectric constant polyaniline/epoxy composites via in situ polymerization for embedded capacitor applications. *Polymer* 48:1510–1516. doi:10.1016/j.polymer.2007.01.057
- Marcel C, Tarascon JM (2001) An all-plastic WO₃-H₂O/polyaniline electrochromic device. *Solid State Ionics* 143:89–101. doi:10.1016/S0167-2738(01)00837-2
- Mathew H, Vrinda S, Kuriakose PS, SyamalaKumari B, Manuel A (2013) Synthesis and electrical characterization of polyaniline-multiwalled carbon nanotube composites with different dopants. *Int J Sci Res Publ* 8:1–10
- Meroufel A, Deslouis C, Touzain S (2008) Electrochemical and anticorrosion performances of zinc-rich and polyaniline powder coatings. *Electrochim Acta* 53:2331–2338. doi:10.1016/j.electacta.2007.09.056
- Mooss VA, Athawale AA (2016) Polyaniline-graphene oxide nanocomposites: Influence of nonconducting graphene oxide on the conductivity and oxidation-reduction mechanism of polyaniline. *J Polym Sci A Polym Chem* 54:3778–3786. doi:10.1002/pola.28277
- Mostafaei A, Nasirpouri F (2014) Epoxy/polyaniline–ZnO nanorods hybrid nanocomposite coatings: Synthesis, characterization and corrosion protection performance of conducting paints. *Prog Org Coat* 77:146–159. doi:10.1016/j.porgcoat.2013.08.015
- Navarro CG, Meyer JC, Sundaram RS, Chuvilin A, Kurasch S, Burghard M, Kern K, Kaiser U (2010) Atomic structure of reduced graphene oxide. *Nano Lett* 10:1144–1148. doi:10.1021/nl9031617
- Olad A, Naseri B (2010) Preparation, characterization, and anticorrosive properties of a novel polyaniline/clinoptilolite nanocomposite. *Prog Organic Coating* 67:233–238. doi:10.1016/j.porgcoat.2009.12.003
- Pimenta MA, Dresselhaus G, Dresselhaus MS, Cancado LG, Jorio A, Saito R (2007) Studying disorder in graphite-based systems by Raman spectroscopy. *Phys Chem Chem Phys* 9:1276–1291. doi:10.1039/B613962K
- Radhakrishnan S, Siju CR, Mahanta D, Patil S, Madras G (2009) Conducting polyaniline–nano-TiO₂ composites for smart corrosion resistant coatings. *Electrochim Acta* 54:1249–1254. doi:10.1016/j.electacta.2008.08.069
- Rana U, Malik S (2012) Graphene oxide/polyaniline nanostructures: transformation of 2D sheet to 1D nanotube and in situ reduction. *Chem Commun* 48:10862–10864. doi:10.1039/C2CC36052G

- Rohwerder M, Michalik A (2007) Conducting polymers for corrosion protection: what makes the difference between failure and success? *Electrochim Acta* 53:1300–1313. doi:[10.1016/j.electacta.2007.05.026](https://doi.org/10.1016/j.electacta.2007.05.026)
- Sahoo S, Khurana GS, Barik K, Dussan S, Barrionuevo D, Katiyar RS (2013) In situ Raman studies of electrically reduced graphene oxide and its field-emission properties. *J Phys Chem C* 117:5485–5491. doi:[10.1021/jp400573w](https://doi.org/10.1021/jp400573w)
- Samui AB, Patankar AS, Rangarajan J, Deb PC (2003) Study of polyaniline containing paint for corrosion prevention. *Prog Org Coat* 47:1–7. doi:[10.1016/S0300-9440\(02\)00117-0](https://doi.org/10.1016/S0300-9440(02)00117-0)
- Sathiyarayanan S, Muthukrishnan S, Venkatachari G (2006) Performance of polyaniline pigmented vinyl acrylic coating on steel in aqueous solutions. *Prog Org Coat* 55:5–10. doi:[10.1016/j.porgcoat.2005.09.002](https://doi.org/10.1016/j.porgcoat.2005.09.002)
- Sawangphruk M, Suksomboon M, Kongsupornsak K, Khuntilo J, Srimuk P, Sanguansak Y, Klunbud P, Suktha P, Chiochan P (2013) High-performance supercapacitors based on silver nanoparticle–polyaniline–graphene nanocomposites coated on flexible carbon fiber paper. *J Mater Chem A* 1:9630–9636. doi:[10.1039/C3TA12194A](https://doi.org/10.1039/C3TA12194A)
- Shao D, Hou G, Li J, Wen T, Ren X, Xinagke, Wang (2014) PANI/GO as a super adsorbent for the selective adsorption of uranium (VI). *Chem Eng J* 255:604–612. doi:[10.1016/j.cej.2014.06.063](https://doi.org/10.1016/j.cej.2014.06.063)
- Stankovich S, Pine RD, Chen X, Wu N, Nguyen SBT, Ruoff RS (2006) Stable aqueous dispersions of graphitic nanoplatelets via the reduction of exfoliated graphite oxide in the presence of poly(sodium 4-styrenesulfonate). *J Mater Chem* 16:155–158. doi:[10.1039/B512799H](https://doi.org/10.1039/B512799H)
- Valles C, Muñoz PJE, Benito AM, Maser WK (2011) Simultaneous reduction of graphene oxide and polyaniline: doping-assisted formation of a solid state charge-transfer complex. *J Phys Chem C* 115:10468–10474. doi:[10.1021/jp201791h](https://doi.org/10.1021/jp201791h)
- Venugopal G, Krishnamoorthy K, Mohan R, Kim S (2012) An investigation of the electrical transport properties of graphene oxide thin films. *Mater Chem Phys* 132:29–33. doi:[10.1016/j.matchemphys.2011.10.040](https://doi.org/10.1016/j.matchemphys.2011.10.040)
- Wang W, Gumfekar SP, Jia Q, Zhao B (2013) Ferrite-grafted polyaniline nanofibers as electromagnetic shielding materials. *J Mater Chem* 1:2851–2859. doi:[10.1039/C3TC00757J](https://doi.org/10.1039/C3TC00757J)
- Wessling B (1996) Corrosion prevention with an organic metal (polyaniline): Surface ennobling, passivation, corrosion test results. *Mater Corros* 47:439–445. doi:[10.1002/maco.19960470804](https://doi.org/10.1002/maco.19960470804)
- Williams G, McMurray HN (2005) Factors affecting acid-base stability of the interface between polyaniline emeraldine salt and oxide covered metal. *Electrochem Solid-State Lett* 8:B42–B45. doi:[10.1149/1.1959978](https://doi.org/10.1149/1.1959978)
- Yang D, Lu W, Goering R, Mattes BR (2009) Investigation of polyaniline processibility using GPC/Uv–vis analysis. *Synth Met* 159:666–674. doi:[10.1016/j.synthmet.2008.12.013](https://doi.org/10.1016/j.synthmet.2008.12.013)
- Yeh JM, Chang KC, Hsu MH, Lu HI, Lai MC, Liu PJ, Hsu CH, Ji WF, Chuang TL, Wei Y, Liu WR (2014) Room-temperature cured hydrophobic epoxy/graphene composites as corrosion inhibitor for cold-rolled steel. *Carbon* 66:144–153. doi:[10.1016/j.carbon.2013.08.052](https://doi.org/10.1016/j.carbon.2013.08.052)
- Yu H, Tian Z, Wang L, Saleem M, Ren F, Ren P, Chen Y, Sun R, Sun Y, Huang L (2014). *RSC Adv* 4:28195–28208. doi:[10.1039/c4ra03146f](https://doi.org/10.1039/c4ra03146f)
- Zhang X, Xie D, Zhong L, Cai W, Sheng X (2016) Synthesis of functionalized graphene/polyaniline nanocomposites with effective synergistic reinforcement on anticorrosion. *Ind Eng Chem Res* 55:8576–8585. doi:[10.1021/acs.iecr.6b01975](https://doi.org/10.1021/acs.iecr.6b01975)